New setup for angular distribution measurements of Auger electrons from fixed in space molecules

Article *in* Review of Scientific Instruments · December 2000

DOI: 10.1063/1.1327310

9 authors, including:

Renaud Guillemin
French National Centre for Scientific Research
146 PUBLICATIONS **1,936** CITATIONS

SEE PROFILE

Eiji Shigemasa
Institute for Molecular Science
231 PUBLICATIONS **4,641** CITATIONS

SEE PROFILE

Catalin Miron
Atomic Energy and Alternative Energies Commission
223 PUBLICATIONS **3,463** CITATIONS

SEE PROFILE

Nicolas Leclercq
SOLEIL synchrotron
56 PUBLICATIONS **810** CITATIONS

SEE PROFILE

New setup for angular distribution measurements of Auger electrons from fixed in space molecules

R. Guillemin[a)]
LURE, Bat 209d, Universite Paris-Sud, 91898 Orsay Cedex, France
and CEA/DRECAM/SPAM, CEN Saclay, 91191 Gif/Yvette Cedex, France

E. Shigemasa
UVSOR, Institute for Molecular Science, Myodaiji, Okazaki 444-8585, Japan

K. Le Guen, D. Ceolin, C. Miron, and N. Leclercq
LURE, Bat 209d, Universite Paris-Sud, 91898 Orsay Cedex, France
and CEA/DRECAM/SPAM, CEN Saclay, 91191 Gif/Yvette Cedex, France

K. Ueda
Research Institute for Scientific Measurements, Tohoku University, Sendai 980-77, Japan

P. Morin and M. Simon
LURE, Bat 209d, Universite Paris-Sud, 91898 Orsay Cedex, France
and CEA/DRECAM/SPAM, CEN Saclay, 91191 Gif/Yvette Cedex, France

(Received 2 June 2000; accepted for publication 28 September 2000)

A new experimental setup for measurement of the angular distributions of energy selected Auger electrons emitted from fixed in space molecules is presented. The system is based on two identical ion detectors with a small angular acceptance placed at 0° and 90° relative to the polarization axis of the incident radiation, and a high luminosity double-toroidal electron analyzer combined with position sensitive detection. This setup allows selection of the molecular alignment for σ and π ionization channels simultaneously and provides an energy and ejection angle measurement of the outgoing electron. The performance in terms of energy and angular resolution, as well as the calibration procedure, are discussed. Sample results obtained on the carbon monoxide ionized above the C 1*s* threshold are presented. © *2000 American Institute of Physics.* [S0034-6748(00)01801-9]

I. INTRODUCTION

The understanding of the fundamental processes leading to the molecular dissociation after irradiation motivated numerous experimental studies for about 30 yrs.[1] In this field, angular correlation between ionic fragments and outgoing electrons soon became a point of interest, but has known an important development only recently, thanks to technical improvements that opened up new experimental possibilities. The general theory describing the angular distributions from free molecules was developed about 20 yrs ago by Dill *et al.*[2] They predicted that the molecular absorption can be highly anisotropic both for discrete resonances and in the continuum.[3] Thus, the molecular photoabsorption leads to neutral or ionic states with definite orientations of the molecule. It is then possible, by measuring the ionic emission intensity along a particular direction, to perform an angle-resolved measurement and decompose the conventional photoabsorption spectra into their molecular symmetry components.[4] In pioneering studies, Shigemasa *et al.*[5–7] have investigated the possibility of measuring the angular distributions of photoelectrons from fixed in space molecules and to determine the partial wave contributions in the continuum,[7] dipole transition matrix elements and phase shift differences. To further assess information on molecular structure as well as relaxation and dissociation dynamics of irradiated molecules, the experimental investigation of angular distributions of Auger electrons and ionic fragments is necessary. This topic has motivated recent experimental works for angle-resolved molecular Auger spectroscopy[8–10] using synchrotron radiation, as well as theoretical studies.[11–14] From the experimental point of view, further improvements of apparatus and experimental techniques allow new insights to complete our understanding of angular correlations in molecular relaxation processes. In particular, coincidence techniques using efficient electron spectrometers together with a position sensitive detection furnish experimental possibilities of hitherto inaccessible multi-angle measurements as presented in Ref. 15 with a double-toroidal analyzer and in Ref. 16 with a cylindrical mirror analyzer, both equipped with a position sensitive detector. The experimental setup presented here has been developed for coincidence measurements of angle-selected ionic fragments and energy and angle resolved outgoing electrons. It provides a new tool for efficient measurements of angular distributions of energy selected Auger electrons, emitted by fixed in space molecules in the gas phase.

[a)]Author to whom correspondence should be addressed; electronic mail: guillemin@lure.u-psud.fr

II. PRINCIPLE AND GENERAL CONSIDERATIONS

Technical advances in synchrotron radiation and monochromator technologies now provide a very selective and narrow bandwidth for x-ray excitation. Thus, it is possible to cause molecular core excitation along particular resonances to excited states, unoccupied orbitals, or ionic states, continuum shape resonance. The electronic decay of a core-excited state, namely resonant Auger decay, taking place in a neutral system, and the normal Auger decay occurring in ionic systems are both described by Coulomb matrix elements. The former process, induced by a primary excitation below the ionization threshold, leads either to one-hole final states when the excited electron is involved in the decay (participator decay) or two-hole one-electron final states (spectator decay) when the excited electron does not participate

$$AB+h\nu \rightarrow AB^{*} \rightarrow AB^{+(*)}+e^{-}_{\text{Auger}}.$$

The second process, following molecular photoionization, leads to two-hole or two-hole one-electron states of doubly charged ions

$$AB+h\nu \rightarrow AB^{+}{}^{*}+e^{-}_{\text{Photo}} \rightarrow AB^{++(*)}+e^{-}_{\text{Auger}}+e^{-}_{\text{Photo}}.$$

Following the bonding or anti-bonding character of the final state, the molecule will or will not subsequently dissociate.

When the exciting radiation is linearly polarized, the probability of photoabsorption by the molecule depends on its orientation relatively to the polarization axis.[3] Within the dipole approximation, the selection rules allow only $\Delta\Lambda = 0, \pm 1$ transitions. For a transition from an initial state to an excited state with same Σ symmetry, we have $\Delta\Lambda = 0$ and the probability of absorption is maximum for a molecular orientation parallel to the electric vector. For a transition from an initial state with a Σ symmetry to an excited state with a Π symmetry, $\Delta\Lambda = \pm 1$ and the probability is maximum perpendicular to the electric vector. For a transition induced in a sample of randomly oriented diatomic molecules by a linearly polarized radiation, the probability law to absorb the incoming light is given by the Cooper-Zare equation

$$\frac{d\sigma(h\nu,\theta)}{d\Omega} = \frac{\sigma(h\nu)}{4\pi}\left[1+\frac{\beta_m(h\nu)}{4}(1+3\mathcal{P}_1\cos 2\theta)\right] \quad (1)$$

describing the photoabsorption cross section as a function of the angle θ between the molecular axis and the **E** vector of the incident light. $\mathcal{P}_1$ is the first Stokes parameter representing the degree of linear polarization of the light. The asymmetry of the molecular orientation is characterized by the so-called asymmetry parameter β_m which is photon energy dependent. Thus, β_m can be directly determined from ion angular distribution by measuring the difference between the photoabsorption strengths parallel and perpendicular to the polarization axis.[17–19] Considering now the electron angular distribution, the same equation (1) also describes the differential photoionization cross section by replacing β_m by β_e. The β_e parameter is the electron anisotropy parameter and contains interference terms between σ and π ionization amplitudes, which are not present in β_m. The angle θ is then measured between the polarization axis of the light and the momentum vector of the ejected electron. By measuring the angular distribution of photoelectrons from randomly oriented molecules with respect to the polarization axis, one can measure β_e as a function of the photon energy. The angular distribution of Auger electrons is likewise described by Eq. (1) by replacing β_m by a parameter β which is the product of the molecular asymmetry parameter β_m and the intrinsic anisotropy parameter $\mathcal{C}_a$.[2] $\mathcal{C}_a$ is characteristic of each Auger transition and independent of the photon energy. β_m extends from -1, orientation perpendicular to the electric vector, through 0, no orientation, to 2, orientation parallel to the electric vector. As the differential cross section has to be non-negative, $\mathcal{C}_a$ is restricted to the range -0.5 to 1. From the measurement of the angular distribution of Auger electrons relative to the polarization axis, one can deduce the intrinsic anisotropy parameter of a selected Auger transition.[10]

Moreover, by measuring the electronic emission from fixed in space molecules, one does not only have access to the anisotropy of the transitions and the symmetry of the involved states, but also directly to the harmonic composition of the angular distribution, which depends on the orbital momentum of the Auger electron. This may be studied in the gas phase taking into account the ''axial recoil approximation.''[20] Since the lifetime of the molecular core excited state is much shorter than the typical molecular rotation period, it can be considered that the dissociation occurs before rotation. The direction of the emitted fragment ion is thus considered to be equivalent to the molecular orientation at the time of the absorption. It is then possible to select the momentum of the transition by an angle-selected detection of the energetic fragment ions produced by the subsequent dissociation of the molecule and to find out the orientation of the internuclear axis at the time of the photon absorption. Moreover, if one can measure the angular distribution of the electrons in the laboratory frame and detect in coincidence an energetic fragment ion in a selected direction, we can deduce from the coincidence measurement the angular distribution of the electrons in the molecular frame. As a direct consequence, the measurements are restricted to angular distributions of dissociative states that produce energetic fragments.

III. EXPERIMENTAL SETUP

The experimental setup has been developed at LURE, and the experiments have been carried out on the SA22 beam line supplying the synchrotron radiation emitted from a bending magnet of the SuperACO positron storage ring. This beam line provides photons in the 100–920 eV range with a resolving power up to 5000. The synchrotron radiation is monochromatized by a 12 m grazing incidence monochromator, combining four interchangeable plane gratings and a spherical refocusing mirror. The light is focused through a rotational feedthrough at the center of the interaction region (Fig. 1). It crosses an effusive gas beam formed by expansion through a monocapillary of 200 μm diameter. The gas inlet

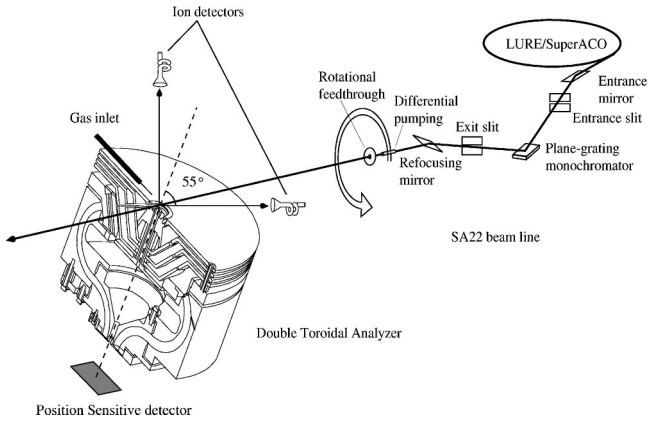

FIG. 1. Schematic representation of the experimental setup at the output of the SA22 beam line of SuperACO.

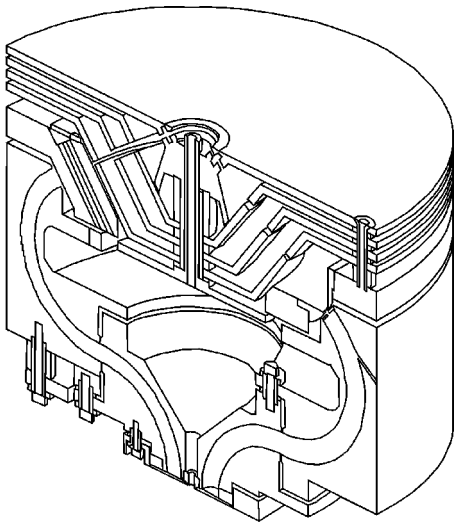

FIG. 2. Three-dimensional cut of the DTA's mechanical setup.

is grounded. Residual magnetic fields are prevented by a double μ-metal shielding and care is taken not to use any magnetic material in the chamber. The base pressure is 10^{-7} Torr and increases to 10^{-5} Torr in the presence of the target gas. A differential pumping section is placed between the experimental chamber and the beam line to avoid any pressure rise in the beam line. The whole chamber is rotatable around the direction of photon propagation, *Y* axis.

A. Ion detectors

Since our goal is only to detect energetic ions in a selected direction, we opted for a very simple detection scheme for the ions, using the same design as reported in Ref. 5. We use two identical ion detectors with retarding field, based on two commercial channeltrons used in pulse counting operating mode. Three molybdenum meshes are placed in front of the entrance cone of the channeltrons. The first one faces the ionization region and is grounded. On the second one, we apply a positive retarding field in order to detect only energetic ions. The third one is also connected to ground to avoid field penetration from the entrance of the channeltron on which we apply -2200 V. The mesh holders are made from molybdenum and also serve as diaphragms, in order to limit the angular acceptance. Each detector has a collection half angle of 3.5°. The front part of the detector is covered by a truncated cone connected to ground and the whole detector is fixed in a grounded box to avoid electric fields in the ionization region. According to the dipole selection rules, one detector is installed at 0° relative to the polarization axis to select $\Sigma \rightarrow \Sigma$ transitions and the other one is at 90° to select $\Sigma \rightarrow \Pi$ transitions. The two detectors are screwed directly on the grounded upper plate of the electron analyzer lens and aligned with respect to the electron analyzer axis as will be seen below.

B. Double toroidal electron analyzer

A high transmission, electrostatic ''double toroidal'' electron energy analyzer (DTA) has recently been developed in the group, as reported in detail elsewhere[21] (represented in Fig. 2). The particular design of this DTA makes it a powerful tool for simultaneous multi-energy and multi-angle detection. The electrons are accelerated or retarded and focused by a four element electrostatic conical lens, on the entrance slit of the analyzer. The electrons are dispersed in energy between double toroidal deflecting plates and focused in the output plane on a position sensitive detector (PSD). The performances of this double toroidal analyzer can be summarized as follows:

(1) a large acceptance angle (5% of 4π);
(2) parallel detection over 12% of the pass energy;
(3) resolving power equal to 1% of the pass energy.

The conical symmetry of the lens only allows the detection of electrons emitted from the source volume at 54.7° relative to the cylindrical symmetry axis of the analyzer. When the analyzer axis and the polarization axis are superimposed, we eliminate any angular dependence and directly measure a signal proportional to the cross section since we are dealing with nearly linearly polarized light. Otherwise, one has to consider the electron emission on the surface of a cone with an aperture angle of 54.7°. This situation is similar to that reported by Wehlitz *et al.*[16] but the angle detection range provided here is wider as we discuss below. In the following considerations, we assume that the light is linearly polarized, the dipole approximation is valid and the molecule is diatomic. To describe the emission we need to consider two coordinate systems. One is relative to the molecular frame; one is relative to the laboratory frame defined by the analyzer axis. In Fig. 3, the laboratory coordinate system (X,Y,Z) (black arrows) is chosen so that the *Z* axis corresponds to the analyzer axis and the *Y* axis corresponds to the photon propagation axis. The electron ejection is described using the Eulerian polar angle ζ (not shown in figure) and the azimuthal angle ϕ.

The molecular coordinate system (x,y,z) (white arrows) is chosen so that the *z* axis corresponds to the molecular axis, and the *y* axis also corresponds to the photon propagation axis (y and Y are superimposed). The electron emission is described using the Eulerian polar angle θ and the azimuthal angle χ (not shown in figure). As we consider the emission within the dipole approximation, one only needs the polar angle θ to describe the electron emission in the (x,z) plane

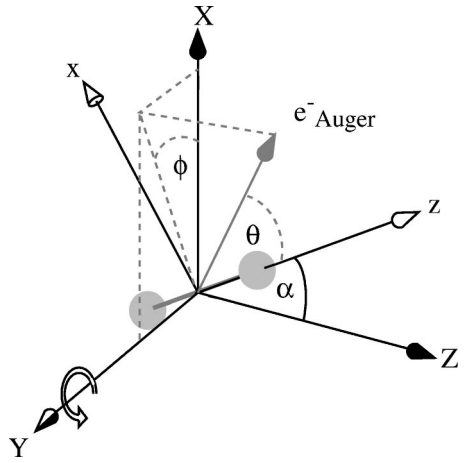

FIG. 3. Schematic diagram of the two frames: molecular frame (white arrows) and laboratory frame (black arrows).

of the molecular frame. We allow the molecular frame to rotate around the *Y* axis relative to the laboratory axis. The angle α on the figure describes this rotation.

The angle θ can be expressed as

$$\theta = \cos^{-1}(-\sin\zeta \sin\alpha \cos\phi + \cos\zeta \cos\alpha). \quad (2)$$

Taking into account the geometry of the analyzer, the laboratory polar angle ζ is fixed to 54.7°; ϕ is the angle of detection on the PSD imaging system. Based on Eq. (2), one can deduce that when the analyzer axis and the polarization axis are superimposed together with the molecular axis, we can only measure the emission at the angle $\theta = 54.7°$ and thus eliminate the angular dependence. On the other hand, when the angle α is set to 54.7°, one can measure a wide angular range relatively to the molecular coordinate system. If we consider the molecules oriented at 0° with respect to the polarization axis, detected by the ion detector set at 0°, the detection range is extended from 0° to 109.4° and the equation giving θ is

$$\theta = \cos^{-1}(\tfrac{2}{3}\cos\phi + \tfrac{1}{3}). \quad (3)$$

If we consider the molecules oriented at 90° with respect to the polarization axis, and the ion detector set at 90°, the detection range is extended from 20° to 90° and the equation giving θ is

$$\theta = \cos^{-1}\left(\frac{\sqrt{2}}{3} - \frac{\sqrt{2}}{3}\cos\phi\right). \quad (4)$$

We choose this configuration for the experimental setup by setting one detector at 55° and the other one at 35° relative to the analyzer's axis and by rotating the whole chamber to set them at 0° and 90°, respectively, with respect to the polarization axis. The main point here is that because we measure the angular distribution in the molecular frame, the angular ranges deduced for both orientations and the transformation equations from ϕ to θ are different. The angle range 0°–109.4° relative to the polarization axis, obtained here, has to be compared with the angle range 47.7°–132.3° reported by Wehlitz *et al.*,[16] considering that a complete angular description is provided by angles between 0° and 90°.

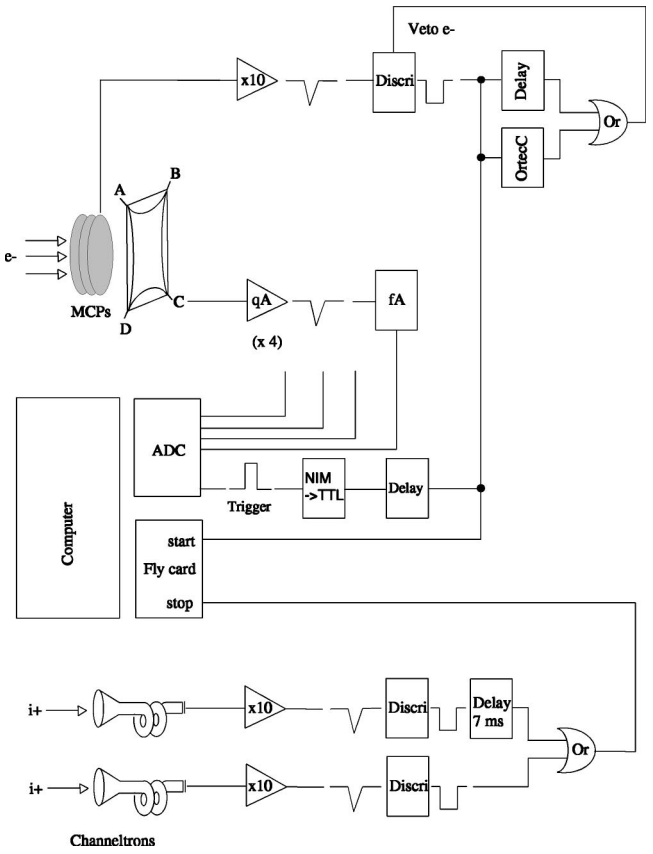

FIG. 4. Schematic representation of the data acquisition system.

C. Position sensitive detector

The detection system placed in the output plane of the DTA is constituted of three 40-mm-diam active area microchannel plates (MCPs) and a two-dimensional resistive anode (from Quantar Technology Inc.). To improve the resolution the front side of the first MCP is biased to the same voltage as the entrance slit corresponding to the average potential of the toroidal plates. A positive high voltage is applied across the MCPs via a *R* divider. The position sensitive detector (PSD) uses a positive charge division method, in which the centroid position of the output cloud is detected; thus the resolution is not influenced by the charge spreading. The charge cloud is divided linearly in proportion to the four corners of the anode depending on the relative (x,y) position of impact. The four signals are amplified using charge preamplifiers outside the vacuum chamber and connected to the data acquisition system. The (x,y) coordinates are computed and converted in (r,ϕ) coordinates.

D. Coincidences

The acquisition cycle, Fig. 4, is triggered by the rear side MCP signal, and the electron part is the same as previously described.[21] The four PSD signals are shaped and digitized by an analog-to-digital converter (ADC) board plugged into the computer. In addition, a veto loop is applied to the trigger signal. The coincidence acquisition system is based on a multi-hit time-to-digital-converter (TDC) system using the MCP signal as a start and the detection of an ion as a stop. A logic gate is used to inhibit the electron signal during the

time necessary for the TDC to operate via a delay, and to synchronize the two ADC and TDC boards. The output signals from the channeltrons are amplified by charge preamplifiers and shaped by fast discriminators. One channel is delayed by 7 μs with respect to the second one and they are mixed afterwards in order to treat all the events on a single TDC channel. Dead time constraints of the electronics impose a limited coincidence rate. However, the main limitation is related to the physical conditions of the experiment, imposed by the detection of correlated events in sharp selected space directions. Indeed, the counting rate in coincidence mode is very low, as shown below. Every valid event is computed as (x,y) electron impact position and stored together with the time information issued by the TDC. We use the commercial software Igor Pro © (from Wavemetrics) for the data acquisition and data handling. A homemade Igor extension allows us to display the spectra and PSD images in real time. This feature is useful for controlling all the experimental parameters, as well as performing the data analysis.

IV. TESTS AND CALIBRATION

A. DTA calibration

After possible offset corrections, the electron impact positions are computed as (r,ϕ) coordinates. The radial distance from the center, r coordinate, corresponds to the varying transmitted energy of the particle reaching the PSD after energy dispersion through the analyzer. It depends on the initial kinetic energy, on the retarding or accelerating voltage of the entrance slit and on the pass energy of the analyzer. The ϕ coordinate is the emission azimuthal angle in the laboratory coordinate system, related to the emission angle θ in the molecular frame by Eq. (3) or (4). The link between the experimental data and the corresponding physical values is provided by an accurate calibration of both intensity and energy dispersion law of the analyzer.

1. Energy calibration

As stated above, the energy window and resolution provided by the DTA are 12% and 1% of the pass energy, respectively. To perform multi-energy and multi-angle measurements, we choose to operate with a pass energy of 80 eV, allowing simultaneous detection of electrons emitted within a 10 eV wide energy range. The DTA dispersion law being nonlinear, we calibrate it by scanning the radial position of a selected electron line as a function of the retarding voltage applied on the DTA's entrance slit with a constant pass energy. The radius to energy correspondence is then obtained by an interpolation curve on the data points and computed for every spectrum. To illustrate the provided resolution, we display in Fig. 5 the argon *LMM* Auger spectrum recorded at 80 eV pass energy and 310 eV photon energy. The energy spectrum is obtained after integration over all ejection angles. The energy scale is calibrated according to Pulkkinen *et al.*[22] By a fitting procedure based on Voigt functions, we measure the full width at half maximum of the lines and deduce the energy resolution for this pass energy. The energy resolution obtained on this spectrum is about 800 meV, which corresponds to 1% of the pass energy. The lifetime broadening has been neglected ($\approx$120 meV) and the five peaks have been considered as isolated lines.

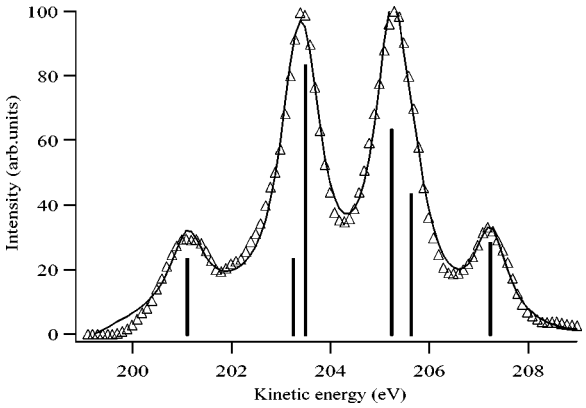

FIG. 5. The argon *LMM* Auger spectrum taken at 80 eV pass energy. The triangles show the experimental data points and the solid line is a fit using Voigt functions based on six isolated lines.

2. Angular calibration

For such imaging systems, the calibration of the angular response of the analyzer is a key point. The final image obtained on the PSD can be affected by several parameters: MCP response, electron trajectory deviation, alignment and source volume effects. Thus, a direct measurement of an angular distribution is not possible. As reported by Duguet *et al.*,[15] the ''spiraling effect'' is a critical point for toroidal analyzers. Because of the nonponctual nature of the source volume, electrons entering the analyzer may have a nonradial velocity component. This causes a constant rotation of the trajectories around the axis of the analyzer and the electrons may arrive on the detector at an angle slightly different from their initial emission angle. This effect appears more significantly when the electrons are retarded before entering the toroid as retardation reduces the radial velocity compared to the azimuthal component. In our setup, it appears to be the main limitation of the angular resolution. The magnitude of this effect is difficult to calibrate, since it depends on the retarding of the electrons. A mechanical misalignment of the electrostatic lens elements can create a nonuniform transmission of the electrons through the analyzer. The extension and the position of the source volume are also critical parameters, thus a very accurate alignment of the photon beam and of the gas capillary with respect to the virtual ''source point'' of the DTA is crucial. This can be achieved by checking the quality of the image displayed in real time together with an optimization of the counting rate for displacements of the photon beam and gas inlet position on a submillimeter scale. On the other hand, the MCPs themselves can introduce some nonuniformity of the detection efficiency due to a long-term fatigue of the channel plates, resulting in a local loss of gain.

a. Angular transmission. It is necessary to calibrate the nonuniformity of the transmission with the measurement of a tabulated distribution. Rare gases are used for this purpose, their angular distribution parameter being tabulated on a large energy range.[23] The photon energy is chosen to select an isotropic angular distribution. The PSD image obtained is used as isotropic reference for further data normalization.

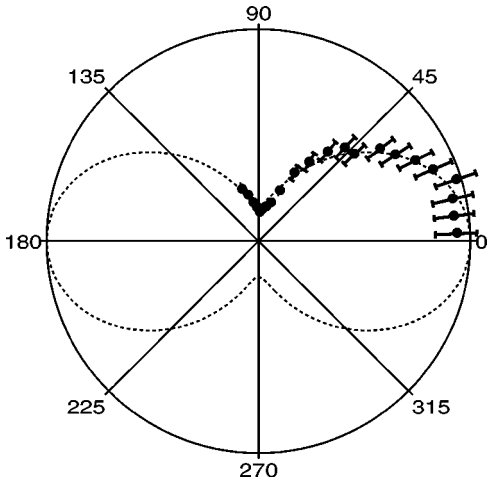

FIG. 6. Angular distribution of N 1*s* photoelectrons from randomly oriented N_2 molecules at $h\nu=490$ eV photon energy. The dots represent the data points. The dashed line is a least-square fit based on Eq. (1) with $\beta_e=2$, and corrected by the polarization degree. The error bars show the statistical error.

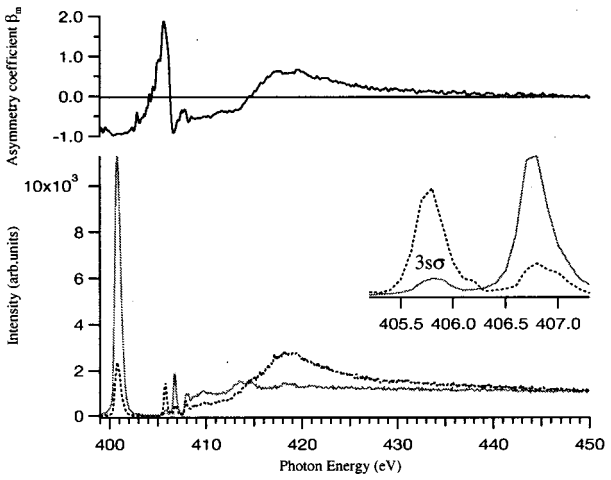

FIG. 7. Symmetry resolved absorption spectrum of N_2 around the 1*s* ionization threshold. The lower graph shows the ion intensities measured by the 0° detector, solid gray line, and by the 90° detector, dashed line. The detail of the $1s\rightarrow 3s\sigma$ transition is shown on the floating graph. The upper graph shows the anisotropy parameter β_m, calculated with the Eq. (5), as a function of the photon energy.

This calibration is done for several retarding voltages on the DTA entrance slit in order to calibrate the angular response over the whole useful radius range of the detector.

b. Angular data analysis. Once the distribution is normalized with respect to the angular transmission, the ϕ angle is transformed in terms of θ angle by the appropriate equation [(3) or (4)]. In the case of noncoincidence measurements, corresponding to randomly oriented molecules, the angle θ is defined with respect to the polarization axis and the relevant transformation is given by Eq. (3). For these measurements, done at relatively low photon energies, we assume that the dipole approximation is valid. It means that the angular distribution is symmetrical with respect to the (y,z) plane. Since the detection is done within a cone, the angular data are redundant on both sides of this plane. So we can add the symmetrical angles after determination of the 0° angle by fitting the data to a known $\beta_e=2$ angular distribution. The summation of the symmetrical angles increases the statistics of the measurement.

c. Angular resolution. As stated above, the spiraling effect is the main source of deterioration in the angular resolution. It is difficult to estimate *a priori*, but can be evaluated *a posteriori* from a well known angular distribution. For instance, Fig. 6 shows the angular distribution of the N 1*s* photoelectrons from randomly oriented N_2 molecules ionized with a photon energy of 490 eV. We use a fitting procedure optimizing both the choice of the 0° angle and the matching with a theoretical curve corresponding to Eq. (1), with an anisotropy parameter $\beta_e=2$, as documented elsewhere.[24] The theoretical curve is corrected by the degree of polarization determined by the ion yield measurements (see below). Within the statistical error, we determine an angular agreement better than 7°. We determined the angular resolution provided by the DTA to be between 5° and 7°. The same resolution is obtained by Duguet *et al.*[15] on a toroidal shaped analyzer. Note that the angular transmission correction is done on a rare gas line with $\beta_e=0$, whereas the angular resolution determination is done on a $\beta_e=2$ line. This insures the consistency of the method.

d. Stability. The measurement of electron angular distributions in coincidence with angle selected ions requires long data acquisition times because of the low coincidence rate inherent to such acquisitions. Over several hours, one can observe slight temperature fluctuations of the mirrors and the grating of the beam line which can affect the beam position at the ionization region. As seen above, an accurate alignment is necessary to achieve reliable measurements. The stability of the system on long time scale must be checked. To eliminate any ambiguities due to a long-term drift of the experimental conditions, we accumulate data on limited times, typically 2 h, calibrating the isotropic reference on a rare gas for each data acquisition, before and after acquisition. Subsequently, in stored data, (x,y) positions and the time of flight are added to increase the statistics of the coincidence measurements.

B. Tests on the ion detectors

1. Determination of the degree of linear polarization

To determine the degree of linear polarization [$\mathcal{P}_1$ in Eq. (1)] provided on the SA22 beam line, we measured the absorption spectrum of N_2 around the 1*s* ionization threshold shown in Fig. 7. The intensities measured by both ion detectors are shown and corrected by the relative detection efficiency of the two detectors. The chosen criterion is the overlap of the two curves far above ($h\nu=450$ eV) the shape resonance maximum lying at 419 eV.[25] The valence contribution has been subtracted. It is then possible to calculate the linear polarization degree using the integral of the peak corresponding to the transition to the $3s\sigma$ Rydberg state which is a pure σ transition with $\beta_m=2$.[26] The corresponding β_m parameter is determined by measuring the difference between the photoabsorption strength parallel and perpendicular to the polarization axis. From Eq. (1), one obtains[27]

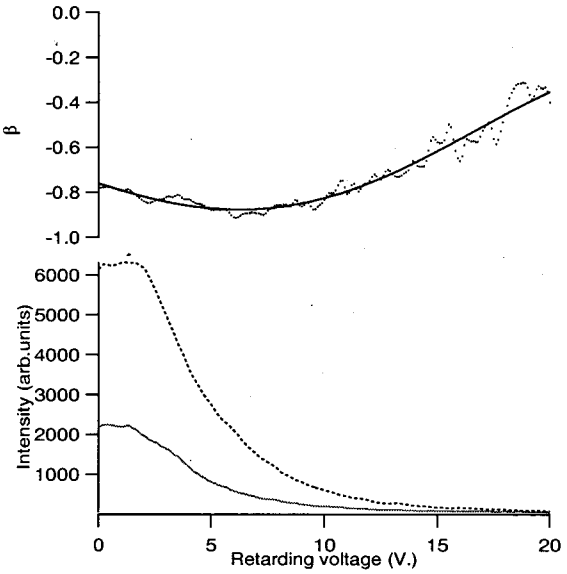

FIG. 8. Influence of the retarding voltage on the measurement of the anisotropy parameter β. The lower graph shows the relative intensities measured at $h\nu = 287.4$ eV on the π^* resonance of CO, with the 0° ion detector (solid line) and the 90° (dashed line) as a function of the retarding voltage. The upper graph shows the corresponding calculated β value as a function of the retarding voltage. The data points are shown as a dashed line and the solid line is a polynomial fitting.

$$\beta_m = \frac{2(\mathcal{I}_\sigma - \mathcal{I}_\pi)}{(\mathcal{I}_\sigma + 2\mathcal{I}_\pi)}, \tag{5}$$

where $\mathcal{I}_\sigma$ is the ion intensity measured at 0° detector and $\mathcal{I}_\pi$ is the intensity measured at 90°. The degree of linear polarization obtained is 89%. This value is in agreement with the expected value from a bending magnet beam line.

2. Choice of the retarding potential

Despite the simplicity of the ion detection system, the choice of the retarding potential applied to select only energetic fragment ions is a key point. It determines indeed the relevance of the axial recoil approximation as well as the ion transmission and so the coincidence counting rate. Saito *et al.*[19] discussed the choice of this potential and its influence on the value measured for the anisotropy parameter. The authors suggest that only ion pairs with high kinetic energy provide information on the molecular orientation at the time of the initial electronic excitation, and a detection of fragments with all kinetic energies results in underestimation of the β_m value. We did check the influence of the retarding potential on the measured β_m value, as shown in Fig. 8, on the example of the C $1s \rightarrow 2\pi^*$ transition of CO at the photon energy of 287.4 eV. The number of detected ions is measured as a function of the retarding potential, at 0° and 90° with respect to the polarization axis. The β_m value plotted in Fig. 8 is calculated from Eq. (5) and corrected for the degree of polarization and the relative transmission of both detectors. In the present detection system, the retarding potential is not directly comparable to the kinetic energy of the fragments. Some field penetration may occur through the meshes which are very close to each other and disturb the retardation

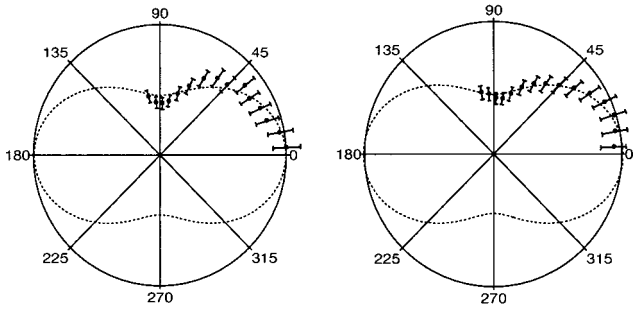

FIG. 9. Angular distribution for the two first participator lines of the resonant Auger decay after $1s \rightarrow \pi^*$ excitation of CO at 287.4 eV of photon energy. The left and right distributions correspond, respectively, to the $CO^+ X\,^2\Sigma^+$ and the $CO^+ A\,^2\Pi$ states. The horizontal axis represents the polarization axis. The filled circles represent the data points. The error bars are the statistical error. The dashed curves are the fits.

effect. As seen in Fig. 8, the β_m value goes to minimum and then increases back as the retarding potential increases. A possible explanation for this behavior is that for low values of the retarding potential, as discussed by Saito *et al.*, we detect slow ions originating from the dissociation through predissociation or tunneling of long lived states for which the molecule has time to rotate before the dissociation occurs. In this case, the alignment information is lost. On the other hand, for high values of the retarding potential, the counting rate is very low and the contribution of the noise and of the adsorbed molecules on the meshes becomes not negligible compared to the real signal from the ionization region. The procedure we adopt is to check the influence of the retarding potential on the β value for each photon energy and choose the potential corresponding to the maximum absolute value of β_m to have the strongest apparent molecular alignment. This choice appears to be an unavoidable compromise between too low retarding potentials involving ions created after valence ionization and too high values dramatically decreasing the counting rate. The same procedure was applied to determine the degree of linear polarization.

V. RESULTS

As an illustration of the capabilities of this new experimental setup, we show here electron angular distribution measurements obtained on the carbon monoxide molecule.

A. Angular distributions from randomly oriented molecules

Figure 9 shows two angular distributions of resonant Auger electrons measured below the C 1*s* ionization threshold, on the top of the $1s \rightarrow \pi^*$ resonance at 287.4 eV photon energy. These distributions are measured without ion coincidence and so represent the angular distributions of Auger electrons emitted after photoabsorption by a sample of randomly oriented molecules with respect to the polarization axis. For the $1s \rightarrow \pi^*$ transition, the asymmetry parameter β_m should, theoretically, be close to -1. The value obtained by our ion measurement is $\beta_m = -0.92(5)$ which is close to the value of -0.95 reported in previous studies.[18,19] The molecules are then preferentially oriented with the internuclear axis perpendicular to the polarization axis. The calcu-

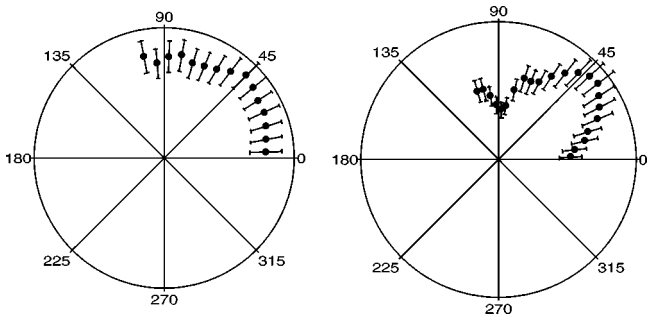

FIG. 10. Angular distributions of Auger electrons emitted from fixed in space CO molecules after $1s\rightarrow\sigma^*$ excitation at 305 eV photon energy. The left and right distributions correspond to the $A\ ^1\Pi$ and $B\ ^1\Sigma$ states of CO^{2+}, respectively. The molecular axis is oriented along the polarization axis and represented by the horizontal axis. The filled circles represent the data points. The error bars indicate the statistical error.

lation of the angular distributions as a function of the angle θ relative to the polarization is done using Eq. (3). The data points are fitted by theoretical curves based on Eq. (1) and taking into account the polarization degree measured for the SA22 beam line. We determine angular anisotropy parameters β of 0.76(8) for the $CO^+X\ ^2\Sigma^+(5\sigma^{-1})$ state and 0.80(8) for the $CO^+A\ ^2\Pi(5\pi^{-1})$ state. These values are in good agreement with those reported previously by Hemmers *et al.*:[10] 0.73(5) and 0.72(5), respectively.

B. Angular distributions in the molecular frame

Figure 10 shows the angular distributions from fixed in space CO molecules of the Auger electrons related to the $CO^{2+}A\ ^1\Pi(5\sigma^{-1}1\pi^{-1})$ final state, centered around 254 eV kinetic energy, and the $CO^{2+}B\ ^1\Sigma(5\sigma^{-1}4\sigma^{-1})$ final state, centered at kinetic energy of 251 eV. The photon energy is set on the top of the $1s\rightarrow\sigma^*$ shape resonance at 305 eV photon energy and the electrons are detected in coincidence with energetic fragment ions emitted at 0° with respect to the polarization axis. Previous studies have shown that the triplet states existing in this energy region have intensities at least an order of magnitude lower than the singlet states considered here.[28] These electronic states are dissociative states leading to the production of both C^+ and O^+ fragments.[29] The time resolution of our ion detection does not distinguish the two atomic fragments, thus we consider here aligned molecules but not oriented ones. The measurement was performed in the experimental conditions reported above and the coincidences counting rate for these measurements was about 2.5 coincidences events per second. The acquisition time was between 6 and 7 h to obtain reliable statistics but the acquisition session provides the measurement of the angular distribution for several Auger lines in coincidence with both ion detectors oriented at 0° and 90°. The contribution of the fortuitous coincidences background to the angular distribution has been subtracted. The angular calibration has been made with the xenon 4*d* photoelectrons at 250 eV photon energy. At this photon energy the anisotropy parameter is tabulated to be 0.[30] The distribution measured for the *A* state is almost isotropic but the one for the *B* state is rich in structure and differs drastically from the usual Auger electron angular distributions from randomly oriented molecules, implying higher momentum components in the angular expansion of the continuum Auger electron wave functions.

VI. DISCUSSION

We believe these results to be the first simultaneous multi-energy and multi-angle measurements of angular distributions of selected Auger transitions from fixed in space molecules. Emphasis is put on the specificity of this experiment which can perform coincidence measurements between ions and high kinetic energy electrons such as Auger electrons. It opens up new possibilities for the investigation of electron angular distributions from fixed in space molecules.

[1] I. Nenner and P. Morin, in *VUV and Soft X-Ray Photoionization*, edited by U. Becker and D. A. Shirley (Plenum, New York, 1996), pp. 291–354.
[2] D. Dill, J. R. Swanson, S. Wallace, and J. L. Dehmer, Phys. Rev. Lett. **45**, 1393 (1980).
[3] J. L. Dehmer and D. Dill, Phys. Rev. Lett. **35**, 213 (1975).
[4] E. Shigemasa, T. Hayaishi, T. Sasaki, and A. Yagishita, Phys. Rev. A **47**, 1824 (1993).
[5] E. Shigemasa, J. Adachi, M. Oura, and A. Yagishita, Phys. Rev. Lett. **74**, 359 (1995).
[6] N. Wanatabe, J. Adachi, K. Soejima, E. Shigemasa, and A. Yagishita, Phys. Rev. Lett. **78**, 4910 (1997).
[7] E. Shigemasa, J. Adachi, K. Soejima, N. Wanatabe, A. Yagishita, G. Raseev, and N. A. Cherepkov, Phys. Rev. Lett. **80**, 1622 (1998).
[8] Q. Zheng, A. K. Edwards, R. M. Wood, and A. M. Mangan, Phys. Rev. A **52**, 3940 (1995).
[9] U. Becker and A. Menzel, Nucl. Instrum. Methods Phys. Res. B **99**, 68 (1995).
[10] O. Hemmers, F. Heizer, J. Viefhaus, K. Wieliczek, and U. Becker, J. Phys. B **32**, 3769 (1999).
[11] Q. Zheng, A. K. Edwards, R. M. Wood, and A. M. Mangan, Phys. Rev. A **52**, 3945 (1995).
[12] K. Zähringer, H.-D. Meyer, and L. S. Cederbaum, Phys. Rev. A **46**, 5463 (1992).
[13] S. Bonhoff, K. Bonhoff, B. Schimmefpfennig, and B. Nestmann, J. Phys. B **30**, 2821 (1997).
[14] S. Bonhoff, K. Bonhoff, and K. Blum, J. Phys. B **32**, 1139 (1999).
[15] A. Duguet, A. Lahmam-Bennani, M. Lecas, and B. El Marji, Rev. Sci. Instrum. **69**, 3524 (1998).
[16] R. Wehlitz, L. S. Pibida, J. C. Levin, and I. A. Sellin, Phys. Rev. A **59**, 421 (1999).
[17] A. Yagishita, H. Maezawa, M. Ukai, and E. Shigemasa, Phys. Rev. Lett. **62**, 36 (1989).
[18] O. Hemmers, F. Heiser, J. Eiben, R. Wehlitz, and U. Becker, Phys. Rev. Lett. **71**, 987 (1993).
[19] N. Saito, F. Heizer, O. Hemmers, K. Wieliczek, J. Viefhaus, and U. Becker, Phys. Rev. A **54**, 2004 (1996).
[20] R. N. Zare, Mol. Photochem. **4**, 1 (1972).
[21] C. Miron, M. Simon, N. Leclercq, and P. Morin, Rev. Sci. Instrum. **68**, 3728 (1997).
[22] H. Pulkkinen, S. Aksela, O.-P. Sairanen, A. Hiltunen, and H. Aksela, J. Phys. B **29**, 3033 (1996).
[23] U. Becker and D. A. Shirley, in Ref. 1, pp. 135–179.
[24] D. W. Lindle, C. M. Truesdale, P. H. Kobrin, T. A. Ferret, P. A. Heimann, U. Becker, H. G. Kerkhoff, and D. A. Shirley, J. Chem. Phys. **81**, 5375 (1984).
[25] E. Shigemasa, K. Ueda, Y. Sato, T. Sasaki, and A. Yagishita, Phys. Rev. A **45**, 2915 (1992).
[26] K. Lee, D. Y. Kim, C. I. Ma, D. A. Lapiano-Smith, and D. M. Hanson, J. Chem. Phys. **93**, 7936 (1990).
[27] J. L. Dehmer and D. Dill, Phys. Rev. A **18**, 164 (1978).
[28] H. Ågren, J. Chem. Phys. **75**, 1267 (1981).
[29] W. Eberhardt, E. W. Plummer, I. W. Lyo, R. Reininger, R. Carr, W. K. Ford, and D. Sondericker, Aust. J. Phys. **39**, 633 (1986).
[30] S. H. Southworth, U. Becker, C. M. Truesdal, P. H. Kobrin, D. W. Lindle, S. Owaki, and D. A. Shirley, Phys. Rev. A **28**, 261 (1983); D. W. Lindle, T. A. Ferret, P. A. Heinmann, and D. A. Shirley, *ibid.* **37**, 3808 (1988); M. Kutzner, V. Radojevic, and H. P. Kelly, *ibid.* **40**, 5052 (1989).